Electronic Supplementary Material (ESI) for Physical Chemistry Chemical Physics.

Supplemental Information for Computation of Overhauser Dynamic Nuclear Polarization processes reveals fundamental correlation between water dynamics, structure, and solvent restructuring entropy

Section A: DNPLab Methodology

Calculation of experimental ODNP parameters is done using the hydration GUI from DNPLab[1]. This tool has been built specifically for data acquired using the home built system in the CNSI facility at University of California Santa Barbara using the 'rb_dnp1' command, however, the hydration module from DNPLab can be used generally to process ODNP data using the same methods and equations[1]. The data is first loaded into the GUI using the "Han Lab" button. The data can be processed by selecting the "Auto Process" button or by clicking through each NMR experiment manually by selecting the "Next" button. The manual process allows the user to change the window width, window center, and phase manually (**Figure S1**). After the enhancements are processed, the inversion recovery NMR experiments are processed and fit to acquire $T1$ at each microwave power in the same manner (**Figure S2**). At the end the GUI will output all the ODNP parameters after inputting the spin concentration, ${T1}_0(0)$ time (sample with no paramagnetic label and at zero power) and magnetic field (**Figure S3**). The results can then be saved.

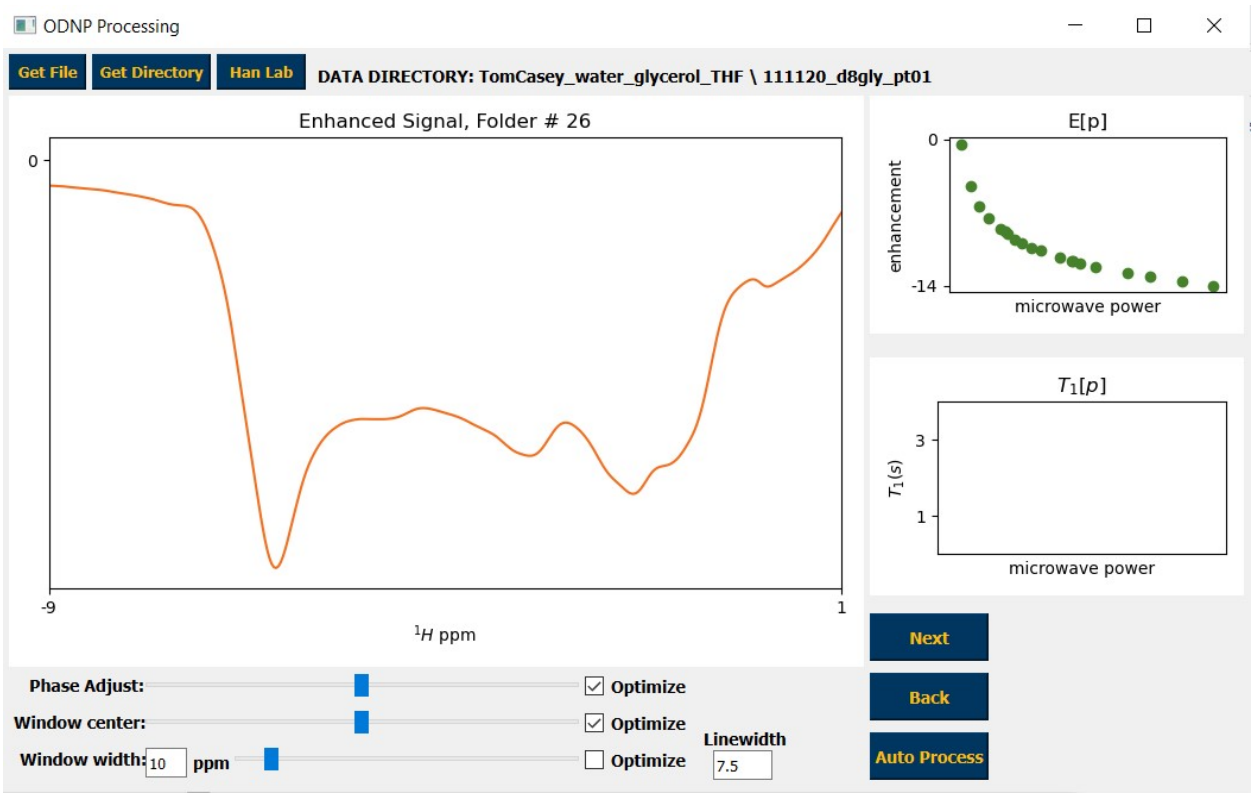

Figure S1. Screenshot of Hydration GUI tool from DNPLab. This image represents the process of NMR integration to calculate the enhancement series.

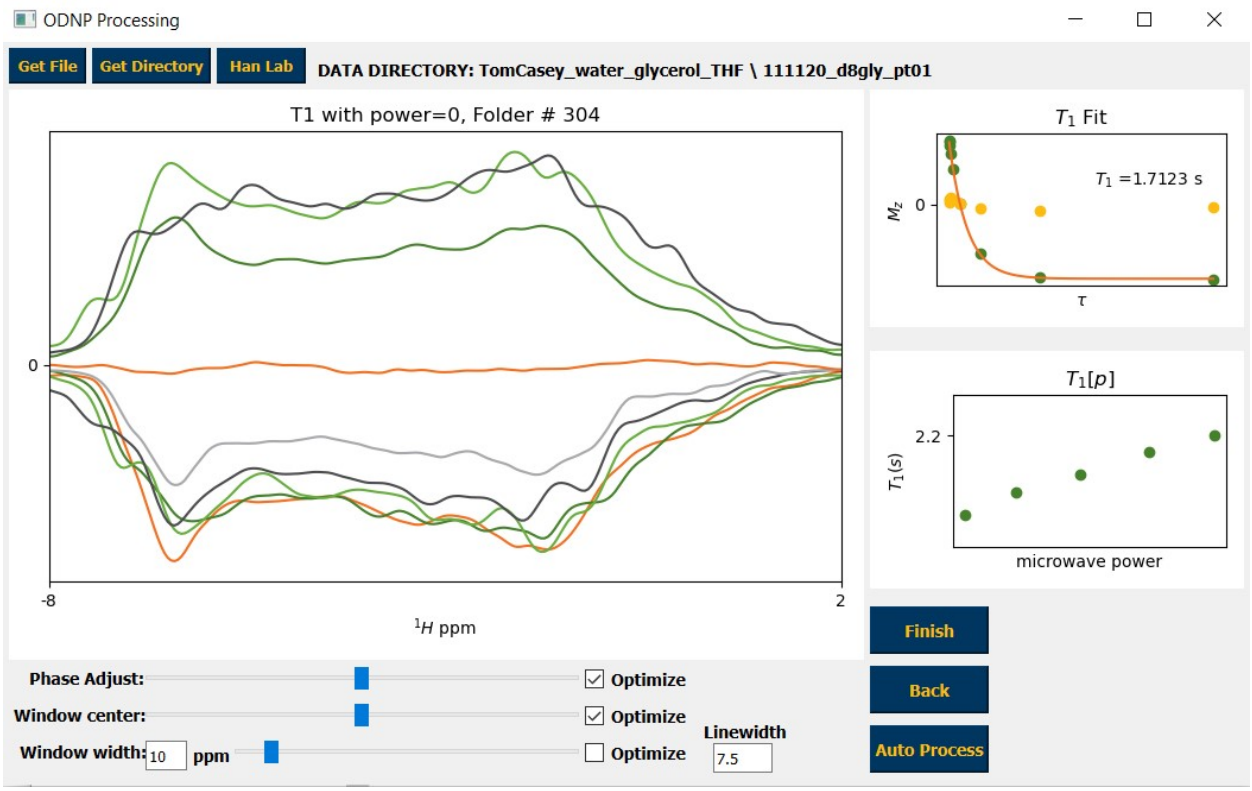

Figure S2. Screenshot of Hydration GUI tool from DNPLab. This image represents the process of inversion recovery experiments to calculate the $T1$ series.

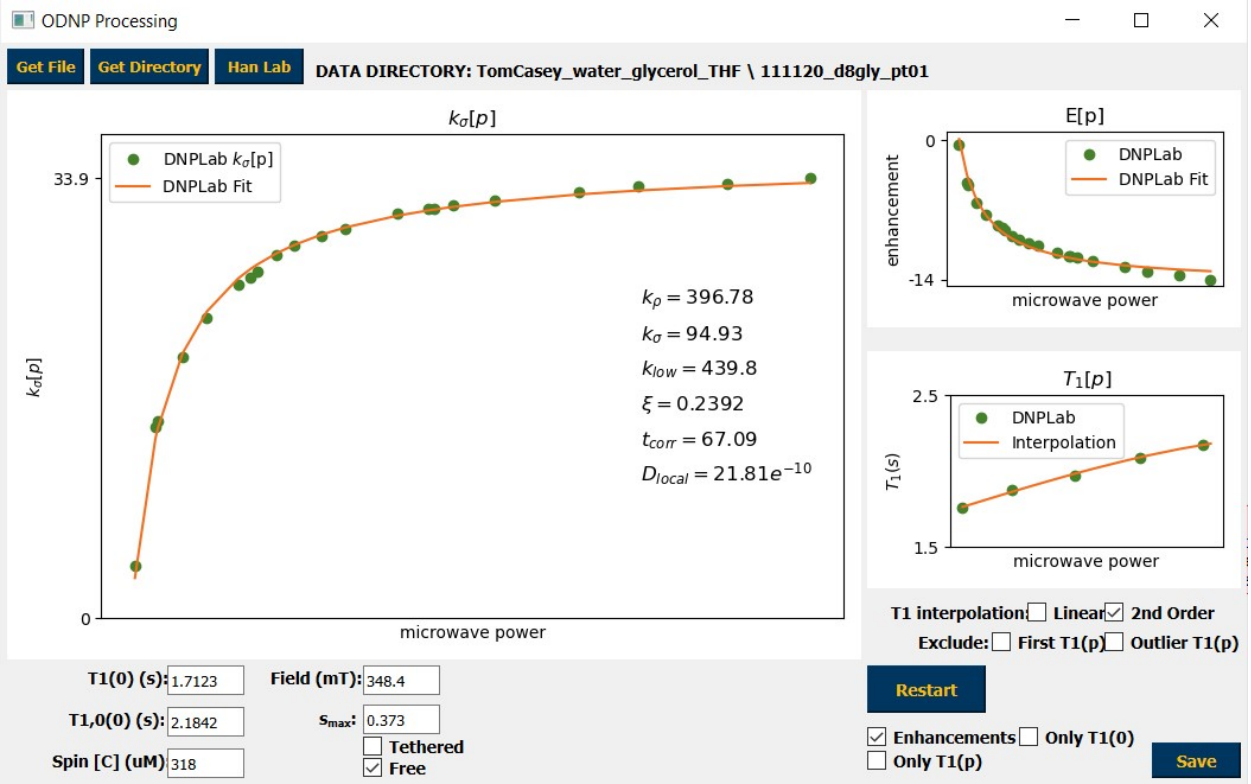

Figure S3. Screenshot of Hydration GUI tool from DNPLab. This image represents the process of calculating the ODNP output parameters.

Section A: EPR Analysis

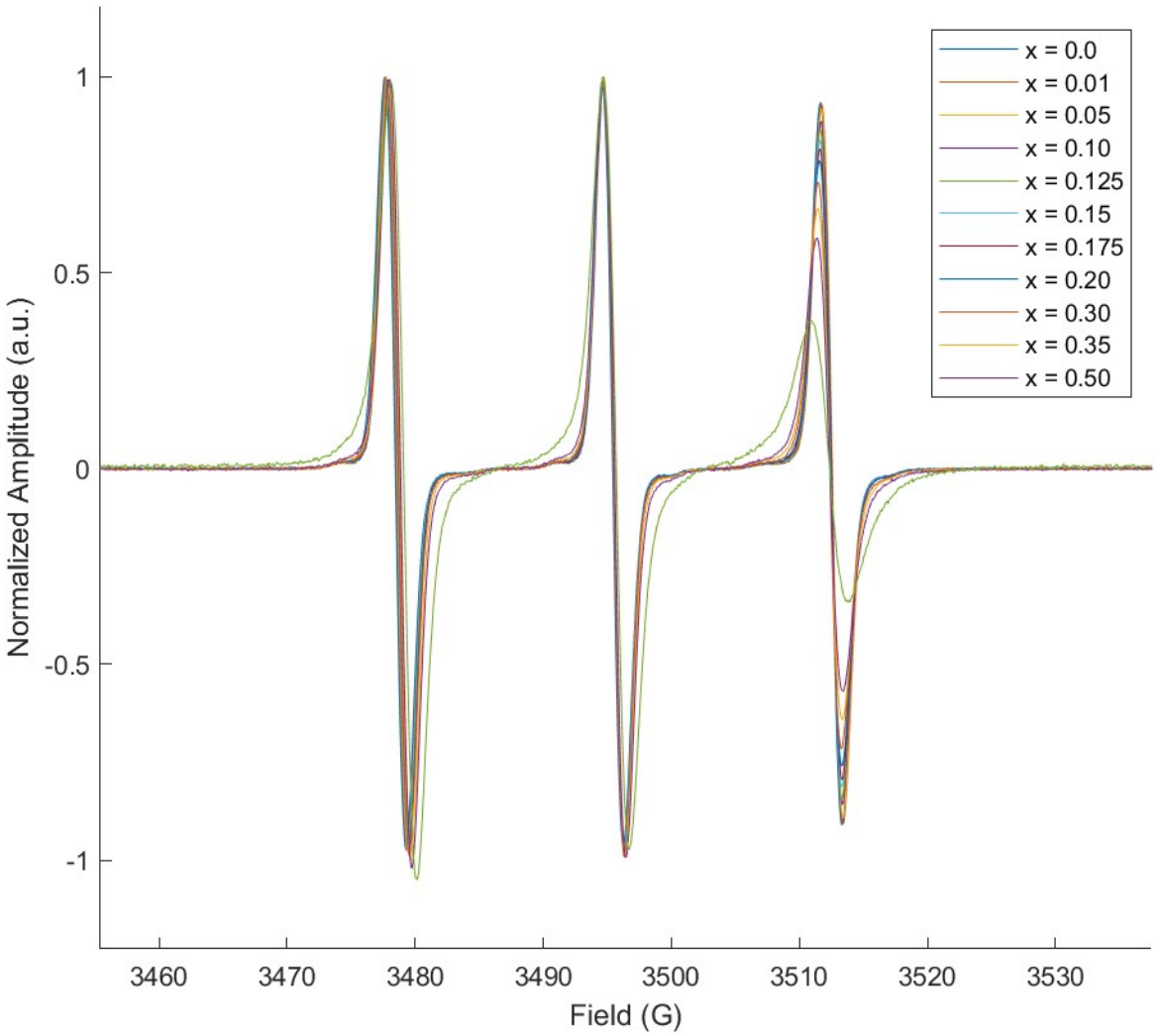

Figure S4. Experimental cwEPR spectra of mixtures of water, glycerol, and TEMPOL. Each curve represents a different glycerol mole fraction, x. The signal amplitude are normalized by the center peak. The high field peak displays an amplitude reduction as glycerol content increases, indicative of slower spin label rotational dynamics, which is expected given the increase in solution viscosity.

Section C: Consideration of the maximal saturation factor

In the analysis of ODNP data, calculation of the coupling factor and cross-relaxation rate, k_σ, requires knowledge of the electron spin saturation factor, $s(p)$. Its value depends on the microwave power, p, and reaches a maximal value, s_{max}, between $\frac{1}{3}$ and 1 for ^{14}N nitroxides at high power. s_{max} depends on two key mechanisms: Heisenberg exchange between colliding nitroxide molecules and the longitudinal relaxation of the nitroxide's nitrogen nuclear spin[2–4]. For tethered spin probes, s_{max} maybe assumed to be ≈ 1 because of the faster ^{14}N relaxation; for free spin labels, Heisenberg exchange dominates the value of s_{max} and its value depends on the spin concentration, and generally following predictions by Türke and Bennati[2,4,5]. In this study, for mixtures of water, glycerol, and free TEMPOL as used in this study, determination of s_{max} is nontrivial: it likely is not a value of unity, yet also does not follow the predictions of Türke and Bennati due to the incorporation of glycerol. In our analysis, we do not assume any model and calculate the coupling factor and k_σ relative to bulk taking $s_{max} = 1$.

Section D: Further Details on spectral density calculations

Mathematical Form of the Spherical Harmonic Functions. As stated in the main text, we calculate the spectroscopic quantities ξ, k_σ and $T_{1,0}[0]$ via a time autocorrelation function of the form

$$C^{(m)}(t) = < F_2^{(m)*}(\vec{r}(t)) F_2^{(m)}(\vec{r}(0)) > = \frac{\sum_i^N F_l^{(m)*}(\vec{r}_i(t)) F_l^{(m)}(\vec{r}_i(0))}{\sum_i^N F_l^{(m)*}(\vec{r}_i(0)) F_l^{(m)}(\vec{r}_i(0))}$$

where spherical harmonic functions $F_l^{(m)}(\vec{r}(t))$ are

$$F_2^{(0)}(r(t)) = \sqrt{\frac{3}{2}}\frac{\left(r^2 - 3r_z^2\right)}{r^5},$$

$$F_2^{(1)}(r(t)) = 3\frac{r_z\left(r_x + ir_y\right)}{r^5},$$

and

$$F_2^{(2)}(r(t)) = -\frac{3\left(r_x - ir_y\right)^2}{2\quad r^5}.$$

For ξ and k_σ, N and $\vec{r}_i(t)$ are the number of water hydrogens in the simulation box and the displacement vector between the *4-Hydroxy-TEMPO* radical oxygen and the i-th water hydrogen at time t, respectively. In the case of $T_{1,0}[0]$, N and $\vec{r}_i(t)$ are the number of water hydrogens in the simulation box (excluding the randomly chosen probe hydrogen) and the displacement vector between the probe water hydrogen and the i-th water hydrogen at time t, respectively.

Concentration dependence of the spectral density amplitudes. As shown indirectly in **Figure 3(a)** in the main text, we find that the spectral density functions at the Larmor precession frequency of the spin probe radical election $J^{(m)}(\omega_S)$ exhibits non-monotonic behavior as glycerol concentration increases. On the contrary, the spectral density functions at the precession frequency of a water proton $J^{(m)}(\omega_I)$ increases monotonically with glycerol concentration.

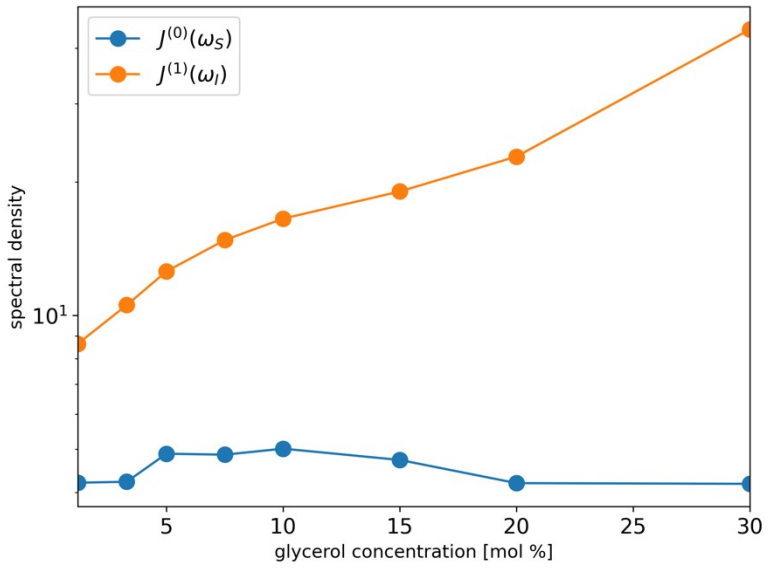

Figure S5. Comparing the amplitude of spectral density functions at ω_S (blue) and ω_I (orange) as a function of glycerol concentration. Amplitudes of the form $J^{(m)}(\omega_I)$ dominate across the entire range of concentrations, reducing the sensitivity of ξ to the non-monotonicity of amplitudes of the form $J^{(m)}(\omega_S)$.

Increase in the relative error of estimating long time behavior of $C_{ODNP}^{(m)}$. As discussed in the main text, we fit the ODNP autocorrelation functions to a tri-exponential model function

$$C_{ODNP,fit}^{(m)} = a_1^{(m)} e^{-t/\tau_1^{(m)}} + a_2^{(m)} e^{-t/\tau_2^{(m)}} + (1 - a_1^{(m)} - a_2^{(m)}) e^{-t/\tau_3^{(m)}}$$

where $\tau_1^{(m)} > \tau_2^{(m)} > \tau_3^{(m)}$.

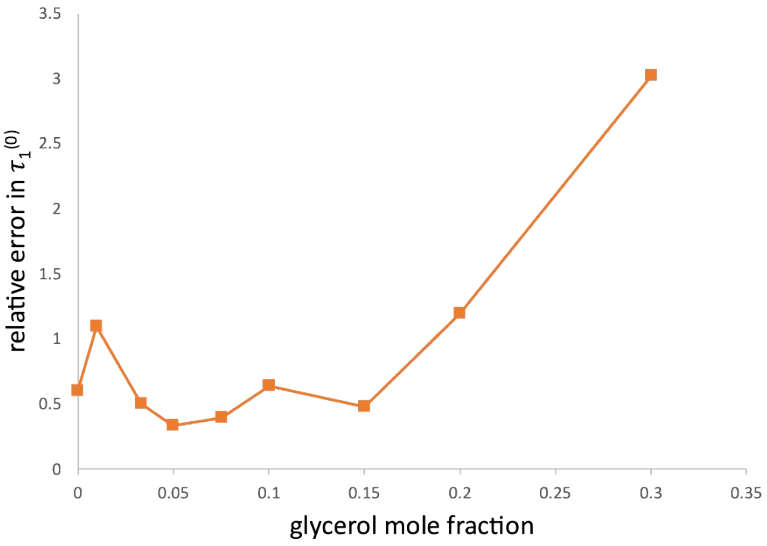

Figure S6. The relative error in the long timescale fitting parameter $\tau_1^{(0)}$ for the 0-th order ODNP correlation function $C_{ODNP,fit}^{(0)}$ increases dramatically for glycerol mole fractions higher than 0.15.

Table S1. Tri-exponential fitting function parameters for $C_{ODNP}^{(0)}$ at all simulated mixture compositions. Here, the uncertainties are 95% confidence intervals on the fitting parameters resulting from a bootstrapping procedure.

	$C_{ODNP}^{(0)}$ fitting parameters: $C_{ODNP,fit}^{(0)} = a_1 e^{-t/\tau_1} + a_2 e^{-t/\tau_2} + a_3 e^{-t/\tau_3}$					
x_{glyc}	a_1	a_2	a_3	τ_1/ps	τ_2/ps	τ_3/ps
0.00	$0.21^{+0.12}_{-0.10}$	$0.51^{+0.09}_{-0.09}$	$0.28^{+0.16}_{-0.13}$	$25.18^{+10.61}_{-6.10}$	$5.65^{+1.93}_{-2.23}$	$0.24^{+0.16}_{-0.11}$
0.01	$0.27^{+0.07}_{-0.10}$	$0.50^{+0.07}_{-0.07}$	$0.23^{+0.10}_{-0.12}$	$27.58^{+7.54}_{-4.23}$	$4.90^{+3.61}_{-1.31}$	$0.17^{+0.67}_{-0.09}$
0.033	$0.24^{+0..12}_{-0.14}$	$0.49^{+0.09}_{-0.12}$	$0.27^{+0.15}_{-0.19}$	$36.66^{+29.88}_{-9.91}$	$7.06^{+4.63}_{-3.01}$	$0.30^{+1.02}_{-0.22}$
0.05	$0.29^{+0.08}_{-0.15}$	$0.49^{+0.07}_{-0.07}$	$0.22^{+0.11}_{-0.17}$	$32.66^{+19.94}_{-6.06}$	$5.74^{+4.62}_{-1.52}$	$0.15^{+0.56}_{-0.06}$
0.075	$0.28^{+0.18}_{-0.18}$	$0.46^{+0.20}_{-0.13}$	$0.26^{+0.27}_{-0.22}$	$50.76^{+88.97}_{-16.05}$	$9.46^{+7.05}_{-4.89}$	$0.15^{+0.29}_{-0.08}$

0.10	$0.29^{+0.14}_{-0.16}$	$0.45^{+0.18}_{-0.17}$	$0.25^{+0.23}_{-0.23}$	$58.51^{+19.56}_{-18.78}$	$10.39^{+6.80}_{-3.58}$	$0.29^{+0.63}_{-0.24}$
0.15	$0.32^{+0.13}_{-0.13}$	$0.47^{+0.15}_{-0.14}$	$0.21^{+0.20}_{-0.19}$	$98.46^{+75.27}_{-39.60}$	$10.04^{+10.89}_{-4.96}$	$0.09^{+0.77}_{-0.09}$
0.20	$0.21^{+0.21}_{-0.12}$	$0.55^{+0.15}_{-0.20}$	$0.24^{+0.26}_{-0.23}$	$114.27^{+149.44}_{-45.35}$	$20.54^{+7.59}_{-7.06}$	$0.13^{+0.46}_{-0.12}$
0.30	$0.47^{+0.16}_{-0.29}$	$0.31^{+0.17}_{-0.17}$	$0.21^{+0.23}_{-0.34}$	$139.69^{+133.72}_{-35.17}$	$17.42^{+49.01}_{-11.86}$	$0.11^{+1.88}_{-0.11}$

Table S2. Comparing spectroscopic quantities obtained from ODNP experiments and MD simulations. Here, the MD uncertainties are 95% confidence intervals on the spectroscopic quantities resulting from a bootstrapping procedure. The uncertainties in the experimental values are the result of repeated measurements.

	MD Simulations				ODNP Experiments*		
x_{glyc}	$C_{SL}[mM]$	$k_\sigma/k_{\sigma,bulk}$	ξ/ξ_{bulk}	$T_{1,0}(0)/T_{1,0}($	$k_\sigma/k_{\sigma,bulk}$	ξ/ξ_{bulk}	$T_{1,0}(0)/T_{1,0}($
0.01	26.3	$1.03^{+0.12}_{-0.12}$	$0.97^{+0.12}_{-0.13}$	$0.817^{+0.22}_{-0.22}$	0.37 ± 0.01	0.51	0.87
0.05	22.8	$1.05^{+0.23}_{-0.20}$	$0.76^{+0.13}_{-0.13}$	$0.69^{+0.19}_{-0.16}$	0.40 ± 0.01	0.50	0.73
0.10	19.1	$1.17^{+0.25}_{-0.21}$	$0.59^{+0.14}_{-0.17}$	$0.46^{+0.17}_{-0.13}$	0.47 ± 0.01	0.38	0.60
0.15	16.2	$0.93^{+0.29}_{-0.28}$	$0.36^{+0.13}_{-0.12}$	$0.33^{+0.13}_{-0.10}$	0.53 ± 0.01	0.28	0.48
0.20	13.7	$0.72^{+0.32}_{-0.31}$	$0.28^{+0.22}_{-0.17}$	$0.28^{+0.11}_{-0.13}$	0.59 ± 0.01	0.24	0.40
0.30	10.1	$0.71^{+0.41}_{-0.32}$	$0.10^{+0.07}_{-0.05}$	$0.12^{+0.14}_{-0.08}$	0.66 ± 0.01	0.12	0.26

**The experimental spin-label concentration is held constant 200μM for each glycerol-water mixture.*

Section E: Additional information on MD-derived relaxation time constants

Table S3. Relaxation time constants for $C_{ODNP}^{(0)}(t)$, $C_{survival}(t)$, $C_{OACF}^{(2)}(t)$ *and* $C_{HB}(t)$. Here, the uncertainties are 95% confidence intervals on the fitting parameters resulting from a bootstrapping procedure.

	Relaxation time scales τ_i/ps			
x_{glyc}	$\tau_{ODNP}^{(0)}$	$\tau_{survival}$	τ_{OACF}	τ_{HB}
0.00	$8.22^{+0.67}_{-0.59}$	$14.33^{+0.48}_{-0.37}$	$2.72^{+0.12}_{-0.12}$	$6.57^{+0.24}_{-0.22}$
0.01	$9.90^{+1.68}_{-1.03}$	$15.71^{+0.63}_{-0.80}$	$3.07^{+0.21}_{-0.22}$	$7.30^{+0.43}_{-0.44}$
0.033	$12.02^{+2.19}_{-1.68}$	$17.79^{+0.88}_{-0.85}$	$3.68^{+0.21}_{-0.21}$	$8.82^{+0.34}_{-0.38}$
0.05	$14.51^{+3.59}_{-2.68}$	$20.45^{+1.39}_{-1.23}$	$4.54^{+0.57}_{-0.46}$	$10.82^{+1.12}_{-1.04}$
0.075	$18.85^{+6.36}_{-2.69}$	$23.89^{+2.80}_{-2.35}$	$5.64^{+0.98}_{-0.62}$	$12.19^{+1.94}_{-0.89}$
0.10	$21.65^{+5.90}_{-5.48}$	$26.98^{+2.26}_{-2.18}$	$6.08^{+0.73}_{-0.63}$	$14.58^{+1.70}_{-2.37}$
0.15	$35.11^{+19.22}_{-10.45}$	$41.17^{+5.70}_{-4.71}$	$10.17^{+1.60}_{-1.34}$	$23.64^{+4.29}_{-2.82}$
0.20	$49.52^{+22.61}_{-17.75}$	$47.10^{+10.45}_{-7.68}$	$12.62^{+2.39}_{-1.74}$	$29.05^{+4.53}_{-4.02}$
0.30	$72.64^{+19.51}_{-16.18}$	$90.17^{+26.43}_{-16.49}$	$24.75^{+4.50}_{-5.31}$	$46.79^{+10.53}_{-7.86}$

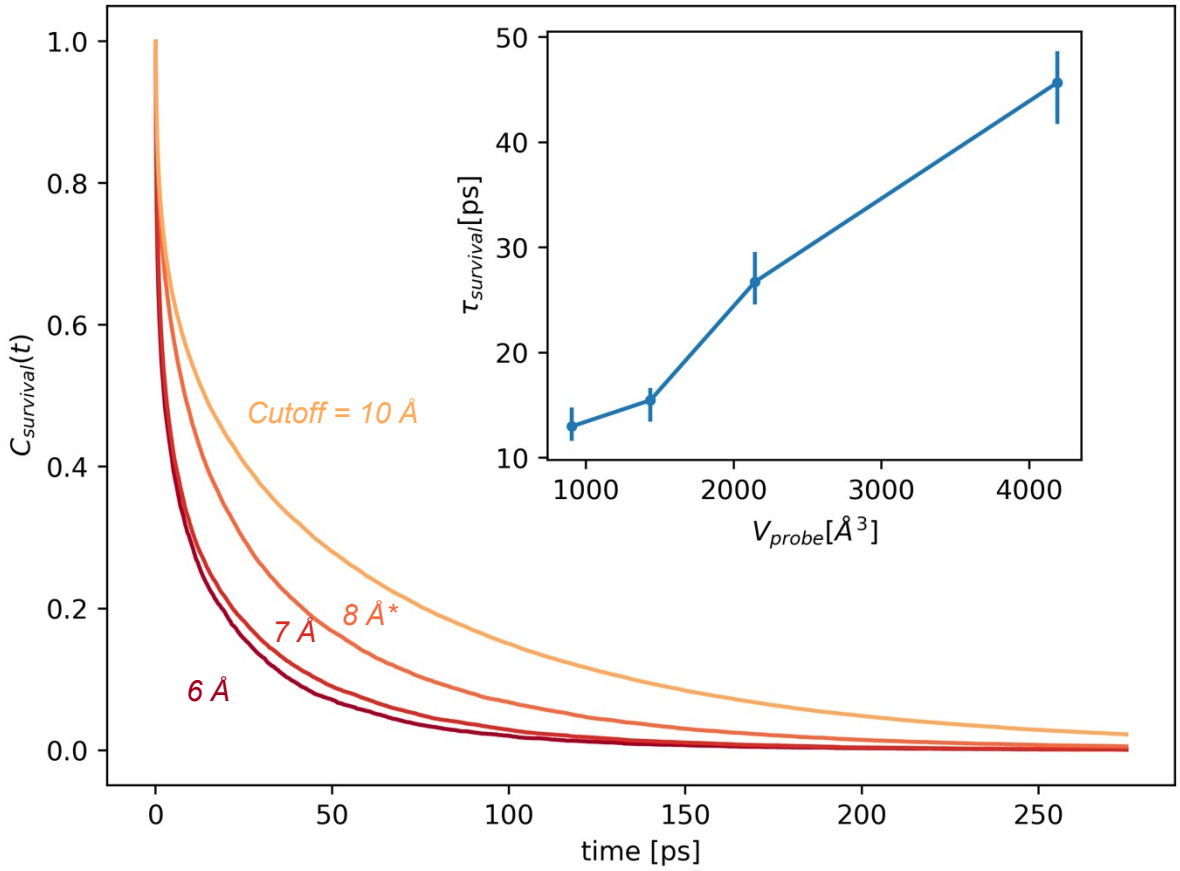

Figure S7. Investigating the effect of cutoff volume on the survival probability calculation for $x_{glyc} = 0.10$. We observe a systematic increase in the decay time for $C_{survival}(t)$ as the cutoff radius from the *4-Hydroxy TEMPO* radical oxygen is increased through values of: 6, 7, 8, and 10 Å. These cutoff radii correspond to spherical cutoff volumes of 904.77, 1436.76, 2144.66, and 4188.79 Å^3, respectively. In the inset plot, we show the monotonic increase in the relaxation timescale $\tau_{survival} = \int_0^\infty C_{survival}(t)dt$ with increasing cutoff volume.

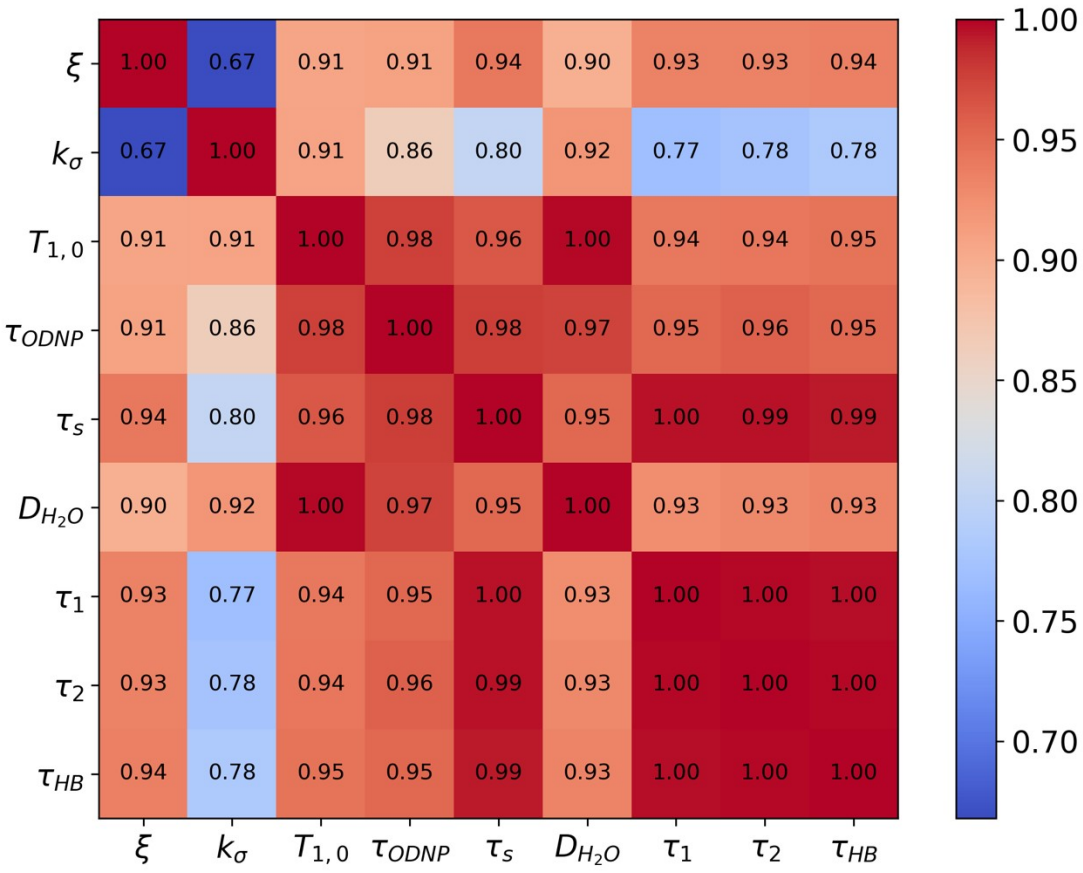

Figure S8. A cross-correlation heat map of all relaxation time constants and measurable dynamics probes. There is excellent correlation between all quantities ($R^2 > 0.9$) except for k_σ.

Section F: Decomposition of ΔG_{solv}^{ex} into solution restructuring, S_{res}, and direct energetic, $\langle U \rangle_{sw}$, terms

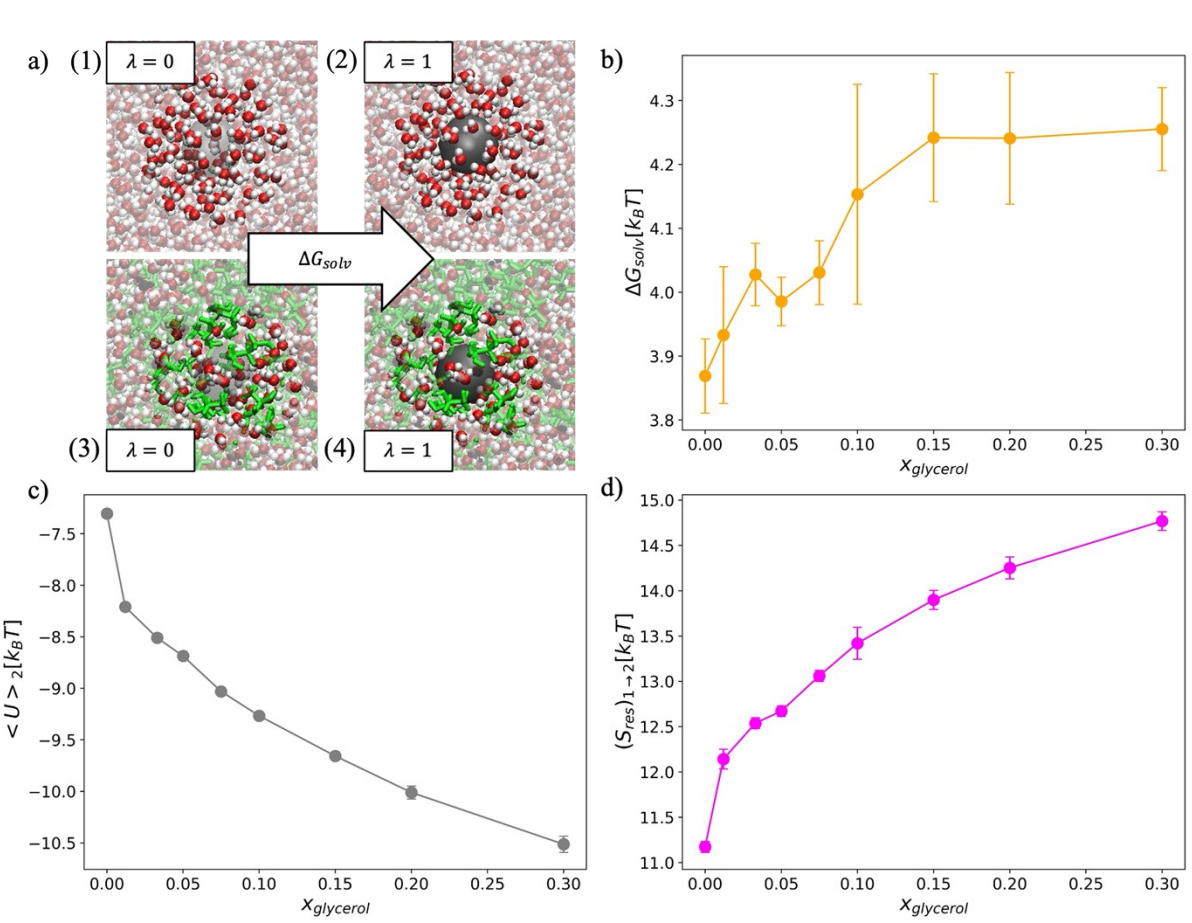

Figure S9: Decomposing the solvation free energy of methane into glycerol-water mixtures. (a) We depict expanded ensemble calculations schematically for glycerol mole fractions of 0 [panels (1) and (2)] and 0.1 [panels (3) and (4)]. The methane molecule is smoothly scaled from a non-interacting $\lambda = 0$ [panels (1) and (3)] to a fully interacting methane molecule $\lambda = 1$ [panels (2) and (4)]. (b) The solvation free energy, ΔG_{solv}, for bringing a methane from vacuum into solution with a glycerol-water mixture shows a non-monotonic trend with increasing glycerol content. The solvation free energy is decomposed into (c) enthalpic contribution via the direct energy

term $< U >_2$ and (d) entropy of solvent restructuring $(S_{res})_{1\to2}$. (c) $< U >_2$ decreases as more glycerol is added to the mixture. (d) $(S_{res})_{1\to2}$ increases as more glycerol is added to the mixture.

References

1. T. Keller, T. Maly, T. Casey, J. M. Franck, Y.-C. Huang, T. R. Webber, Y. Lin and S. Han, DNPLab: Bringing the Power of Python to DNP-NMR Spectroscopy, http://dnplab.net.
2. J. M. Franck, A. Pavlova, J. A. Scott and S. Han, *Progress in Nuclear Magnetic Resonance Spectroscopy*, 2013, **74**, 33–56.
3. B. D. Armstrong and S. Han, *J. Chem. Phys.*, 2007, **127**, 104508.
4. B. D. Armstrong and S. Han, *J. Am. Chem. Soc.*, 2009, **131**, 4641–4647.
5. M.-T. Türke and M. Bennati, *Phys. Chem. Chem. Phys.*, 2011, **13**, 3630–3633.